Climate Dynamics
https://doi.org/10.1007/s00382-021-05934-2

High-resolution dynamical downscaling for regional climate projection in Central Asia based on bias-corrected multiple GCMs

Yuan Qiu[1] · Jinming Feng[1] · Zhongwei Yan[1] · Jun Wang[1] · Zhen Li[1]

Received: 25 February 2021 / Accepted: 11 August 2021

Abstract
Central Asia (CA) is among the most vulnerable regions to climate change due to the fragile ecosystems, frequent natural hazards, strained water resources, and accelerated glacier melting, which underscores the need to achieve robust projection of regional climate change. In this study, we applied three bias-corrected global climate models (GCMs) to conduct 9 km-resolution regional climate simulations in CA for the reference (1986–2005) and future (2031–2050) periods. The regional climate model (RCM) and GCM simulated daily temperature and precipitation are evaluated and the results show that both the bias-correction technique and dynamical downscaling method obtain numerous added values in reproducing the historical climate in CA, respect to the original GCMs. The former contributes more to reducing the biases of the climatology and the latter contributes more to capturing the spatial pattern. The RCM simulations indicate significant warming over CA in the near-term future, with the regional mean increase of annual mean temperature in a range of 1.63–2.01 ℃, relative to the reference period. Pronounced warming is detected north of ~ 45° N in CA from autumn to spring, which can be explained by the snow-albedo feedback. Enhanced warming projected in many mountains in the world is not found in CA, which is consistent with the study based on the reanalysis datasets during the past. Heatwave day frequency, number and maximum duration are expected to become more severe by 2031–2050. Changes in precipitation and Standard Precipitation Index (SPI) shows a wetter condition in CA in the coming decades. However, a fairer assessment of the wet/dry change with Standard Precipitation Evapotranspiration Index (SPEI) which takes into account of both precipitation and potential evapotranspiration reveals a drier condition. The climate change projections presented here serve as a robust scientific basis for assessment of future risk from climate change in CA.

Keywords Regional climate projection · Dynamical downscaling · Bias correction · Central Asia · Near-term future

1 Introduction

Central Asia (hereafter CA), ranging from the Caspian Sea in the west to China in the east and from Russia in the north to Afghanistan and Iran in the south, is consisted of Kazakhstan, Kyrgyzstan, Tajikistan, Turkmenistan, and Uzbekistan, with an area of about 4,000,000 km^2 (Fig. 1a). There are Tien Shan and Pamir mountain ranges in the southeast, the vast grassy steppes of Kazakhstan in the north, and the Kyzylkum and Karakum desert in the south. Located within the Eurasia continent and far from the oceans, this region has arid and semiarid climate with cold winter and hot summer, sparse precipitation, strong potential evaporation, and large annual and daily temperature ranges.

CA has experienced a significant warming (0.16 ℃ per decade) during the past century (1901–2003, Chen et al. 2009), with an accelerating warming rate (0.36–0.42 ℃ per decade) in the past ~ 30 years (1979–2011, Hu et al. 1979), which is detected to be mainly contributed by the anthropogenic forcing, particularly the greenhouse gases forcing (Peng et al. 2019). Meanwhile, a significant increase in annual precipitation was observed in CA (Chen et al. 2011).

The warming and wetting trend in CA has increased both exposure and vulnerabilities to natural hazards, such as heatwaves (Yu et al. 2020; Wang et al. 2020a), landsides, floods, and droughts (Thurman 2011). The World Bank reported that natural disasters lead, on average, to an astounding $10

✉ Jinming Feng
fengjm@tea.ac.cn

[1] Key Laboratory of Regional Climate-Environment for Temperate East Asia (RCE-TEA), Institute of Atmospheric Physics, Chinese Academy of Sciences, Beijing 100029, China

Published online: 18 August 2021

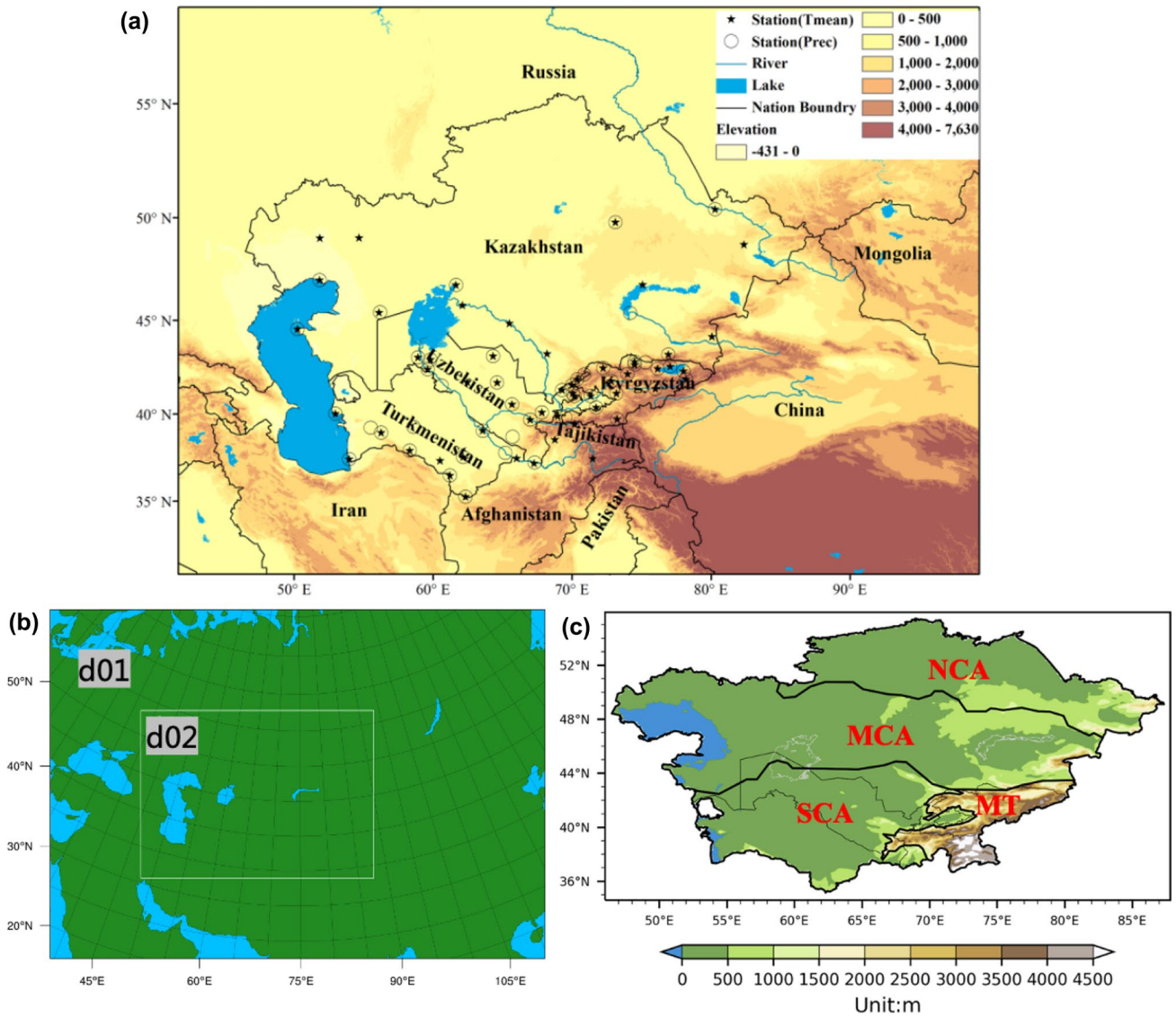

Fig. 1 Study area and its surrounding (**a**), nested domains in the WRF model (**b**), and climate subregions in Central Asia (**c**). In subplot a, stations with records of daily mean temperature (Tmean) and precipitation (Prec) are marked by starts and circles, respectively

billion in estimated economic losses every year (Burunciuc 2020). The cost is very likely to rise in the future. Water is the most precious resource in CA and its use is the most conflict-prone (Frenken 2013). A warming future can aggravate the tensions concerning water allocation between upstream and downstream areas in this region. Climate change has exacerbated the glacier melting in the Tien Shan (Narama et al. 2010). Although in the first instance shrinking glaciers supply ample quantities of water in the form of increased glacier runoff, reduced glacier volume will ultimately result in a decrease in glacier and total runoff and eventually transform glacial-nival runoff regions in the Tien Shan into nival-pluvial regions (Sorg et al. 2012). The local ecosystems are very sensitive to temperature and precipitation changes (Zhang et al. 2016; Seddon et al. 2016; Gessner et al. 2013), which are anticipated to vary dramatically in the coming decades.

Due to the severe climate changes, frequent natural hazards, strained water resources, accelerated glacier melting and fragile ecosystems in CA, it is imperative to project the regional climate change based on emission scenarios for application to vulnerability, impacts, and adaption assessments. Some efforts have been devoted on climate change projections in CA with both global climate models (GCMs) and regional climate models (RCMs). The GCM simulations largely agree on a regionwide precipitation increase in CA by the end of this century (Huang et al. 2014; Jiang et al. 2020a). The RCM simulations by Mannig et al. (2013) and Ozturk et al. (2017) consistently show notable warming in the cold season in northern CA.

A recent study with the use of RCM found hot days and extreme drought events will increase significantly over CA in the future (Zhu et al. 2020).

To date, the studies about climate change projections in CA are still limited relative to its surrounding areas, like East Asia, South Asia and the Mediterranean region (Darmaraki et al. 2019; Kim et al. 2021; Gao et al. 2006; Kumar and Dimri 2018; Niu et al. 2018; Supari et al. 2020; Zittis et al. 2019; Zou and Zhou 2016, 2017). Most of the previous RCM simulations used a single GCM as the lateral boundary conditions (Mannig et al. 2013; Zhu et al. 2020), which harbor high uncertainties in the projected climate changes. Since the terrain in CA is complex, their resolutions (Zhu et al. 2020; Ozturk et al. 2017; Mannig et al. 2013) are still low (≥ 30 km). The present authors carried out a study that involving the dynamical downscaling of three different GCMs (MPI-ESM-MR, CCSM4, and HadGEM2-ES Table 1) for the CA region with an unprecedented horizontal resolution of 9 km, for the first time. As reported in the 1.5 ℃ special report of the Intergovernmental Panel on Climate Chane (IPCC), we are on track to exceed 1.5 ℃ warming between 2030 and 2052 based on the current warming rate, and hence the near-term future projection becomes more critical to human development than that for the end of this century. Nevertheless, climate changes in CA in the near-term future have not been investigated yet. Therefore, the future simulation period is set as 2031–2050 under Representative Concentration Pathway (RCP) 4.5, with the reference period of 1986–2005.

All GCMs suffer from some kinds of bias, which can be problematic for the downscaling applications especially dealing with extreme weather events (Done et al. 2015; Ehret et al. 2012; Liang et al. 2008; Xu and Yang 2012). Thus, a bias-correction technique (Bruyère et al. 2014) is applied in this study to correct the climatology of the GCMs before the regional modeling. Two questions need to be considered:

What added values do the bias-correction technique and the dynamical downscaling method obtain in simulating the local climate in CA respect to the driving GCMs?
What are the basic features of the projected climate changes across the RCM simulations?

The present paper is, therefore, to evaluate the high-resolution climatology of the downscaled results from three GCMs as well as the GCM outputs; and to demonstrate the projected climate changes in the RCM simulations. The remainder of this paper is organized as follows: Sect. 2 describes the data and methods. Model evaluation and projected changes are in Sect. 3. The main results are summarized in Sect. 4.

2 Data and methods

2.1 Bias-correction technique

MPI-ESM-MR (referred as MPI, Table 1), CCSM4 (referred as CCSM), and HadGEM2-ES (referred as Had) from Phase 5 of the Coupled Model Intercomparison Project (CMIP5) are selected to drive the regional model. Since all GCMs suffer from some forms of bias that may propagate down to the RCM outputs, the bias-correction technique developed by Bruyère et al. (2014) is applied in this study to correct the climatology of the GCMs and allow synoptic and climate variability to change.

Six-hourly GCM data in a 25-year base period (1981–2005), as referred as GCM_{BP}, is broken down into the 25-year mean 6-hourly annual cycle ($\overline{GCM_{BP}}$) plus a 6-hourly perturbation term (GCM'_{BP}):

$$GCM_{BP} = \overline{GCM_{BP}} + GCM'_{BP} \quad (1)$$

The ERA-Interim reanalysis data (Dee et al. 2011) as "observations" (Obs) is similarly broken down into the mean annual cycle ($\overline{Obs}$) and a perturbation term (Obs'):

Table 1 Information about the datasets used in the study

Model	Run	Spatial resolution	Temporal resolution	Variables
MPI-ESM-MR	r1i1p1	1.9°× 1.9°	6-hourly	Full
CCSM4	b40.[20th\RCP4.5]. track1.1 deg.012. cam2.h4	0.9°× 1.3°	6-hourly	Full
HadGEM2-ES	r1i1p1	1.3°× 1.9°	6-hourly	Full
CRU TS v4	–	0.5°× 0.5°	Monthly	Tmean/Tmax/Tmin
CPC	–	0.5°× 0.5°	Daily	Tmean/Tmax/Tmin
ERA5	–	0.25°× 0.25°	Daily	Precipitation

In it, "Full" means all the variables required to generate the initial and lateral boundary conditions for the regional model

$$Obs = \overline{Obs} + Obs' \tag{2}$$

The bias corrected GCM data for the base period, GCM^{*}_{BP}, is then constructed by replacing the GCM mean annual cycle ($\overline{GCM_{BP}}$) from Eq. (1) with the *Obs* mean annual cycle ($\overline{Obs}$) from Eq. 2:

$$GCM^{*}_{BP} = \overline{Obs} + GCM'_{BP} \tag{3}$$

Similarly, six-hourly GCM data in a 25-year future period (2026–2050), as referred as GCM_{FP}, is broken down into the mean annual cycle over the base period ($\overline{GCM_{BP}}$) and a perturbation term (GCM'_{FP}):

$$GCM_{FP} = \overline{GCM_{BP}} + GCM'_{FP} \tag{4}$$

The bias corrected GCM data for the future period, GCM^{*}_{FP}, is then constructed by replacing the GCM mean annual cycle over the base period ($\overline{GCM_{BP}}$) with the *Obs* mean annual cycle ($\overline{Obs}$) from Eq. (2):

$$GCM^{*}_{FP} = \overline{Obs} + GCM'_{FP} \tag{5}$$

Equation (3) and (5) are applied to all the variables required to generate the initial and lateral boundary conditions for the regional model: zonal and meridional wind, geopotential height, air temperature, relative humidity, sea surface temperature, mean sea level pressure, and et al.

To date, this bias-correction technique has been applied in numerous studies (Ortiz et al. 2019; Komurcu et al. 2018; Jing et al. 2020; Jayasankar et al. 2018; Chen and Frauenfeld 2016) and was found to largely improve the performance of RCM in simulating the local mean climate and high-impact weathers. Note that the bias-corrected CCSM4 outputs are available on the Research Data Archive (RDA) of University Corporation for Atmospheric Research (UCAR).

2.2 Regional model and experiment design

The Weather Research and Forecasting (WRF, Skamarock et al. 2008) model is used as the regional model to downscale the GCMs. It has a nested domain (Fig. 1b). The outer domain with a 27-km resolution and 290 × 205 grids covers a large Central Asia region (much larger than the CA region as defined and focused in this study), like in the CORDEX project (https://cordex.org/). The inner domain has a high resolution of 9 km and 409 × 295 grids, covering the CA region. The model has 33 levels in the vertical direction with its top fixed at 50 hPa. The physical schemes in the regional model are set based on our previous work about the sensitivity study of different physical parameterizations of the WRF model in simulating the local climate in CA (Wang et al. 2020b). They comprise the Thompson aerosol-aware microphysics scheme (Thompson and Eidhammer 2014), the New Tiedtke cumulus scheme (Zhang et al. 2011), the Yonsei University planetary boundary layer scheme (Hong et al. 2006), the RRTMG shortwave and longwave schemes (Iacono et al. 2008), and the Noah-MP (multi-physics) land surface model (Niu et al. 2011). Spectral nudging with a weak coefficient of 3×10^{-5} is applied in the outer domain (not in the inner one), which relaxes the model simulations of wind, temperature, and moisture toward the driving conditions, and prevents possible model drift over the long-term integration. Despite greenhouse gases and solar constants, the WRF model is modified to consider other external forcing, such as aerosols, volcanoes, and ozone, so as to make its inner external forcing consistent with the driving GCMs. We evaluated the modified WRF model in East Asia and found that using full external forcing improves the regional simulation there (Luo et al. 2020).

The RCM simulations with bias-corrected multiple GCMs (MPI, CCSM, and Had) as the driving data are referred as WRF_MPI_COR, WRF_CCSM_COR, and WRF_Had_COR, respectively (Table 2). The reference simulations are from December 1, 1985 to December 31, 2005 and the future runs are between December 1, 2030 and the end of 2050 under a moderate carbon emission scenario RCP 4.5, which is arguably the most policy-relevant scenario as the Nationally Determined Contributions (NDCs) greenhouse gas emissions framework would produce similar temperatures trajectories (Gabriel and Kimon 2015). A 10-year (December 1, 1985–December 31, 1995) RCM simulation with the original HadGEM2-ES as the driving data is added, which is referred as WRF_Had (Table 2). Comparison between Had, WRF_Had, and WRF_Had_COR will help

Table 2 Experiment design in the study

Experiment name	Simulation duration	ICs and BCs	Use bias correction or not?
WRF_MPI_COR	1986–2005, 2031–2050	MPI-ESM-MR	Yes
WRF_CCSM_COR	1986–2005, 2031–2050	CCSM4	Yes
WRF_Had_COR	1986–2005, 2031–2050	HadGEM2-ES	Yes
WRF_Had	1986–1995	HadGEM2-ES	No

The initial and lateral boundary conditions are referred as "ICs and BCs"

to quantify the contribution of the bias-correction technique and dynamical downscaling method to improving the RCM simulation. The first month in each simulation is discarded as spin up during the analyses.

2.3 Climate subregions

Various types of terrain and altitude range from 0 to 7500 m above sea level, lead to diverse climates in CA, which underscores the need to do model evaluation and assess the projected climate changes on sub-regions of similar or consistent climate. With the regionalization method used in our previous study (Qiu et al. 2017), the CA region is divided into four climate sub-regions, each of which is coherent in the seasonal circulation pattern in precipitation. They are northern CA (NCA), middle CA (MCA), southern CA (SCA), and the mountainous areas (MT) (Fig. 1c). From NCA to SCA, there is a transition from the cold temperate zone with wet summer to the subtropical zone with dry summer. The annual precipitation is generally below 400 mm in the low-elevation areas (NCA, MCA, and SCA); however, it can exceed 1000 mm in the mountainous areas (MT).

2.4 Observational data

Version 4 of the Climatic Research Unit gridded Time Series (CRU TS v4, Harris et al. 2020, Table 1) is applied to evaluate the simulated daily mean/maximum/minimum temperature (referred as Tmean/Tmax/Tmin) on annual and seasonal scales. CPC (Climate Prediction Center) Global daily temperature from National Oceanic and Atmospheric Administration (NOAA) is used as a supplementary to evaluate the percentiles of the simulated daily temperature. Because the rain-gauge-observation merged in the gridded observations like the CRU dataset is sparse and unevenly distributed over CA, the new generation reanalysis of European Center for Medium-Range Weather Forecasts (ECMWF), i.e., ERA5 (Hersbach et al. 2020) is used as "observations" for precipitation estimation, which has high accuracy in revealing the precipitable water vapor and detecting precipitation events over CA and its surrounding areas (Jiang et al. 2019, 2020b). Before the evaluation, the GCM (RCM) outputs are interpolated to the observations' grids with the bilinear (distance-weighted average) method. We found that both on the annual and seasonal scales, the interpolation methods conserved the area averaged temperature and precipitation in the model outputs with a bias of less than 1–2% between the original and new grids. We thus concluded that our choice of interpolation procedure does not affect the main conclusions of our work.

As the gridded observations (CRU TS v4, CPC, and ERA5) have potential limitations in depicting the climatology of temperature and precipitation in CA, the model outputs are also evaluated with the station observations. The stations' data are from Global Historical Climatology Network (GHCN) of NOAA National Climatic Data Center. They contain monthly mean Tmean from 58 stations (see stars in Fig. 1a) and monthly precipitation from 52 stations (see circles in Fig. 1a), covering the reference period (1986–2005). The stations' data have been quality controlled, and only the stations with less than 20% missing values are selected. Note that a station is compared with the model grid on which it is located.

2.5 Heatwave and drought indices

As the CA region is at high risk from extreme temperatures and drought (Thurman 2011; Yu et al. 2020), it is essential to assess changes in heatwaves and drought in this region. According to Fischer and Schär (2010), a heatwave is defined as a spell of at least six consecutive days with Tmax exceeding the local 90th percentile of the reference period (1986–2005). The 90th percentile is calculated for each calendar day, each model and at each grid point using a centred 15-day-long time window. On the basis of this definition, the following extreme temperature indices are derived for 20-year time slices.

HWF (heatwave day frequency): the average number of days meeting the heatwave criterion per year.

HWN (number of heatwaves): the average number of heatwaves per year.

HWD (heatwave maximum duration): the average duration of the longest heatwave per year (years without heatwaves are excluded from this analysis).

A drought is an event of prolonged shortage in the water supply. In this study, the degree of drought is represented by the Standardized Precipitation Evapotranspiration Index (SPEI, Vicente-Serrano et al. 2010), which is an extension of the widely used Standardized Precipitation Index (SPI, McKee et al. 1993). The SPEI is designed to take into account both precipitation and potential evapotranspiration (PET) in determining drought. Thus, unlike the SPI, the SPEI captures the main impact of increased temperature on water demand. Like the SPI, the SPEI can be calculated on a range of timescales from 1 to 48 months. According to Wei and Wang (2013), the timescale is set as 12 months and PET is estimated with the Thornthwaite method (Thornthwaite 1948). In order to calculate the relative SPEI, the Gamma distribution is utilized and its parameters are first estimated for the reference period (1986–2005). Future drought conditions are then expressed in terms of the present-day climate by computing the relative SPEI for 2031–2050 with respect to the Gamma distribution of the reference period. In order to assess the changes in dry and wet conditions between baseline and future period, the relative SPEI are

compared. To illustrate the contribution of temperature and precipitation changes to the evolution of drought, the relative SPI is also calculated and compared with the relative SPEI. A full description of computation of SPI and SPEI can be seen in Poornima and Pushpalatha (2019).

3 Results

3.1 Added values obtained by the bias-correction technique and dynamical downscaling method

The high-resolution (9 km) downscaled results (WRF_MPI_COR, WRF_CCSM_COR, and WRF_Had_COR) based on bias-corrected multiple GCMs (MPI, CCSM, and Had) are

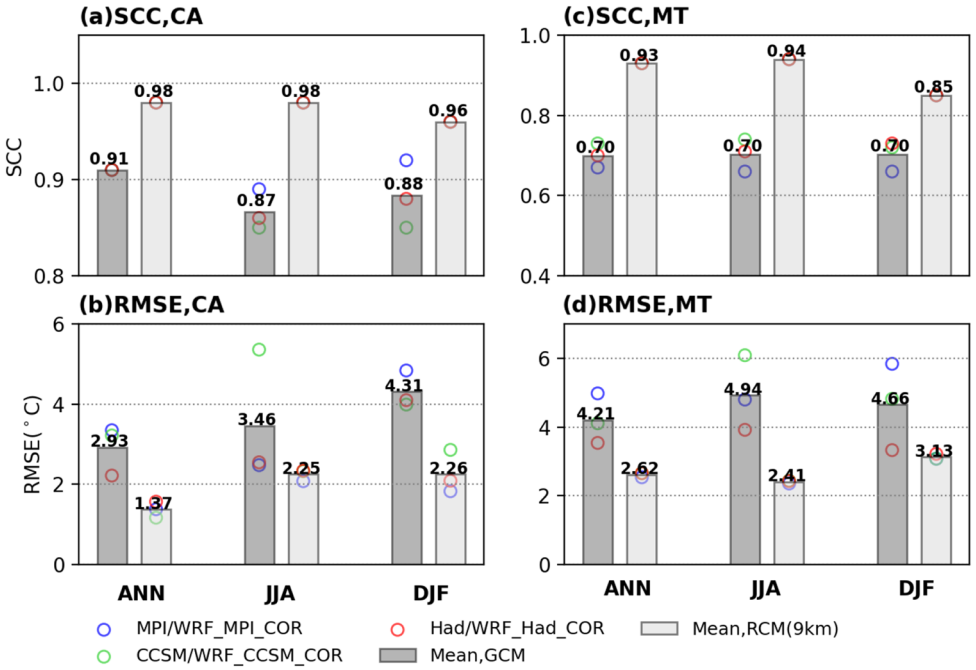

Fig. 2 Spatial correlation coefficients (SCCs) and root mean square errors (RMSEs) of the simulated annual (ANN), summer (JJA, June–July–August), and winter (DJF, December–January–February) mean Tmean over CA and the subregion MT in the GCM (MPI, CCSM, and Had) and RCM (WRF_MPI_COR, WRF_CCSM_COR, and WRF_Had_COR) simulations

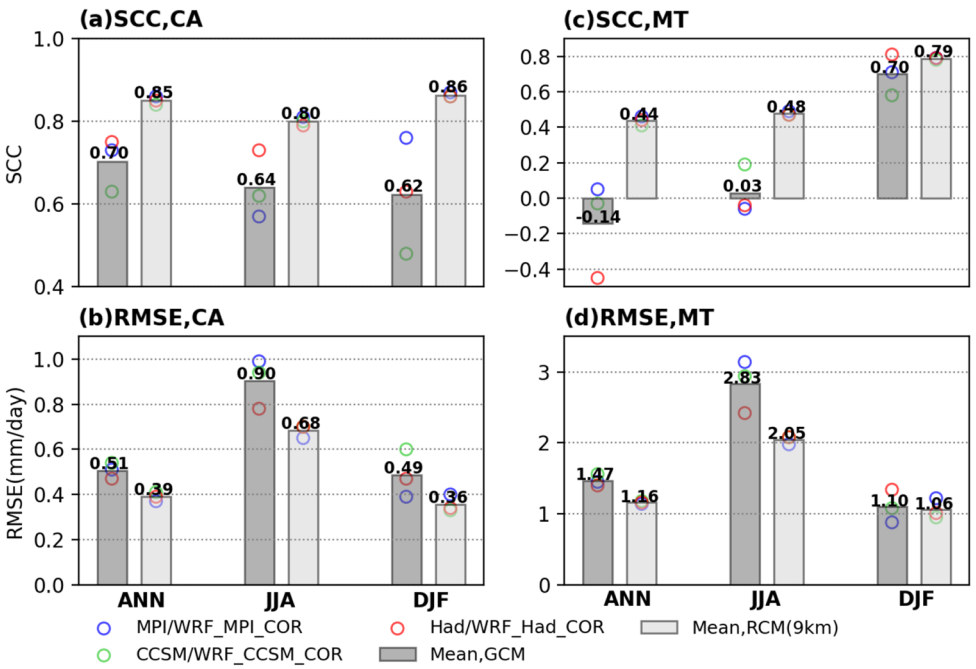

Fig. 3 Same as Fig. 2, but for annual and seasonal precipitation

very close to the observations in simulating the climatology of Tmean and precipitation in CA both on annual and seasonal scales (Fig. S1, Fig. S2, Fig. S3, and Fig. S4). Respect to the driving GCMs, they have numerous added values in simulating the local temperature and precipitation, which is clearly reflected by smaller root mean square errors (RMSEs) and larger spatial correlation coefficients (SCCs, Figs. 2 and 3). For instance, the ensemble-mean RMSEs of annual and seasonal mean Tmean over CA are 1.37–2.26 ℃ in the RCM simulations (Fig. 2b), smaller than those of the GCMs (2.93–4.31 ℃). The ensemble-mean SCCs of annual and seasonal precipitation over CA are 0.80–0.86 in the RCM simulations (Fig. 3a), larger than those of the GCMs (0.62–0.70). The annual and seasonal mean Tmax and Tmin are also evaluated and the results are similar to those of Tmean (not shown here).

The RCM simulations also have added values in simulating the extreme percentiles of daily temperature and precipitation. For instance, the RCMs have excellent performance in simulating all the percentiles of Tmax averaged over CA, NCA, and MCA, with the points on or close to the line of y = x (Fig. S5a-c). The 90th and 95th percentiles of daily precipitation in the RCMs are more realistic than those of the GCMs in the MT region (Fig. S6e).

The added values in simulating the local climate are more pronounced in the mountains than in the whole region (e.g., Fig. 3c vs Fig. 3a). For instance, over the CA region, the SCC of annual precipitation is increased from 0.70 to 0.85 (Fig. 3a); over the MT region, it is increased from -0.14 to 0.44 (Fig. 3c). It highlights the advantages of using dynamical downscaling method in the regions of complex terrain.

The added values discussed above are very likely to be obtained by both the bias-correction technique and dynamical downscaling method. To prove it and furtherly know which contributes more to improving the RCM simulation, the SCCs and RMSEs of precipitation over CA in Had, WRF_Had and WRF_Had_COR during a ten-year period (1986–1995) are compared (Fig. 4). Comparison of Had and WRF_Had shows the contribution of the dynamical downscaling method and comparison of WRF_Had and WRF_Had_COR illustrates that of the bias-correction technique.

The evolution of SCCs and RMSEs (Fig. 4) generally confirms that both the bias-correction technique and dynamical downscaling method bring added values in simulating the local climate in CA. For instance, the dynamical downscaling method increases the SCC of winter precipitation from 0.63 to 0.78 and the bias-correction method furtherly increase it from 0.78 to 0.86 (Fig. 4a). The dynamical downscaling method reduces the RMSE of winter precipitation from 0.56 to 0.50 mm/day and the bias-correction method furtherly reduces it from 0.50 to 0.38 mm/day (Fig. 4b). But it is hard to say which effect contributes more to improving the simulation. The evolution of SCC

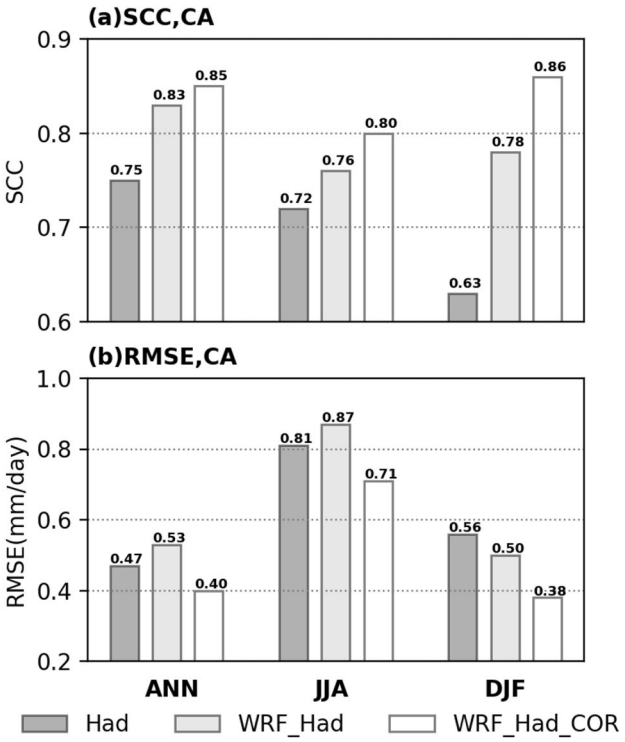

Fig. 4 Spatial correlation coefficients (SCCs) and root mean square errors (RMSEs) of the simulated annual (ANN), summer (JJA, June–July–August), and winter (DJF, December–January–February) precipitation over CA in Had, WRF_Had, and WRF_Had_COR during 1986–1995

shows that the dynamical downscaling method contributes more (Fig. 4a). However, the evolution of RMSE supports the opposite opinion. For instance, the dynamical downscaling method slightly increases the RMSE of annual precipitation over CA from 0.47 to 0.53 mm/day while the bias-correction technique reduces it from 0.53 to 0.40 mm/day (Fig. 4b), offsetting the additional error induced by downscaling.

Figure 5 shows the bias (model minus observation) pattern of annual mean Tmean (1986–1995) in Had, WRF_Had, WRF_Had_COR and the ERI-Interim reanalysis. It's found that the bias pattern of WRF_Had_COR is close to that of the reanalysis dataset (Fig. 5d vs Fig. 5b) instead of the driving GCM (Fig. 5d vs Fig. 5a). The reason is that the ERA-Interim reanalysis as "observation" in the bias-correction procedure comprises the climatology component of the lateral boundary conditions of the regional model and thus the biases of the reanalysis dataset propagate down to the downscaled results based on the bias-corrected GCMs. Without using bias correction, the RCM simulation has similar bias pattern with the driving GCM (Fig. 5c vs Fig. 5a). This finding suggests the use of more state-of-the-art reanalysis dataset like ERA5 in the bias correction in the future so as to make the downscaled results more realistic.

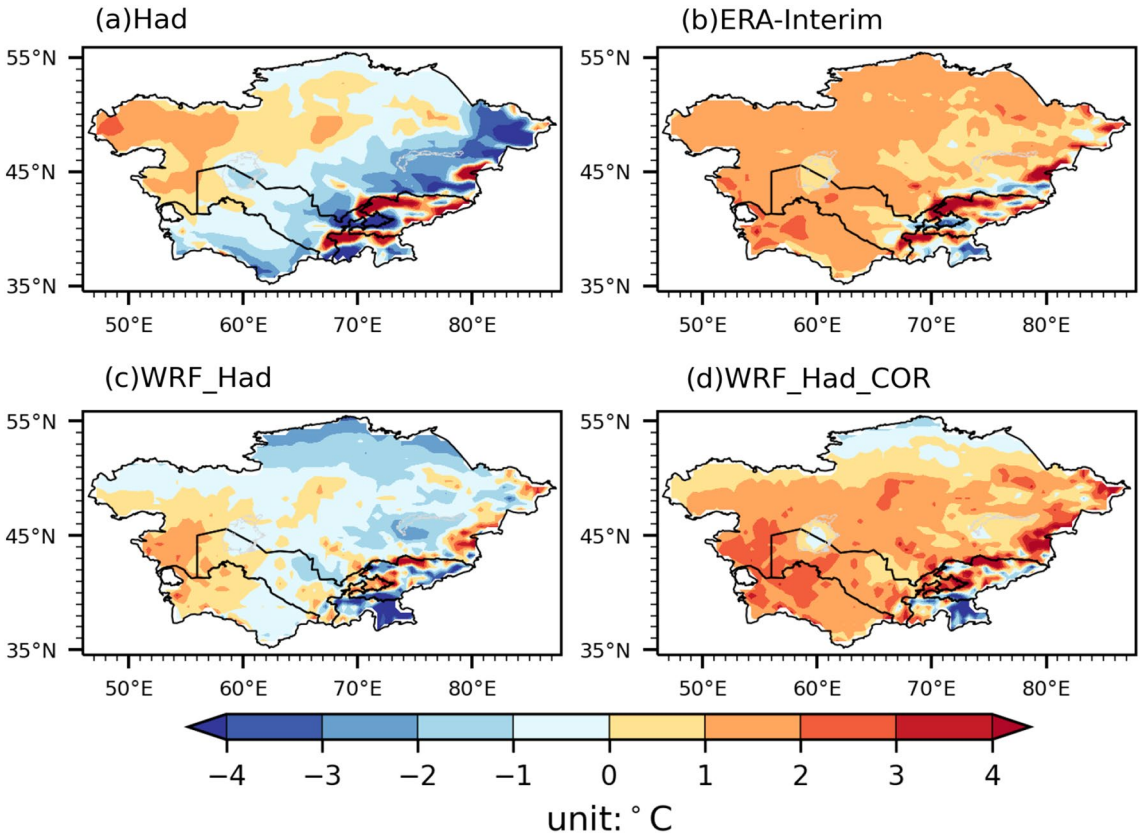

Fig. 5 The bias pattern of annual mean Tmean in Had, WRF_Had, WRF_Had_COR, and the ERA-Interim Reanalysis during 1986–1995

Since the gridded observations (CRU TS v4, CPC, and ERA5) have potential limitations in depicting the climatology of temperature and precipitation in CA, the RCM outputs are also evaluated with the station observations and the results show the RCMs still have a fairly good performance in simulating the local climate. For instance, the simulated annual mean Tmean is very close to the observed, with R^2 as large as 0.86 (Fig. 6a). Though WRF_MPI_COR and WRF_Had_COR overestimated annual precipitation, all the RCMs well captured its spatial pattern, with R^2 in a range of 0.61–0.70 (Fig. 6b).

To sum up, the high-resolution RCMs driven by multiple bias-corrected GCMs are excellent in simulating the local temperature and precipitation in CA despite some systematic biases (e.g., warm (cold) bias during spring and summer (winter)) and obtain substantial added values respect to the original GCMs, which provides a good base for projecting climate changes in CA.

3.2 Basic features of the projected climate changes across the RCM simulations

3.2.1 Warming patterns

All the RCM simulations (WRF_MPI_COR, WRF_CCSM_COR, and WRF_Had_COR) show significant warming over CA in the near-term future (Fig. S7), with the annual mean Tmean increase averaged over the entire area by 1.63, 1.89, and 2.01 ℃, respectively. Though the warming amplitude varies across them, they consistently project the most pronounced mean annual warming north of ~ 45°N in CA (above 2.0 ℃, Fig. 7 and Fig. S7), where subregion NCA and MCA mainly occupy (Fig. 8). Previous simulations projected a notable warming in the northern part of CA in winter (Mannig et al. 2013; Ozturk et al. 2017; Peng et al. 2019). However, the strong warming in the north is also detected

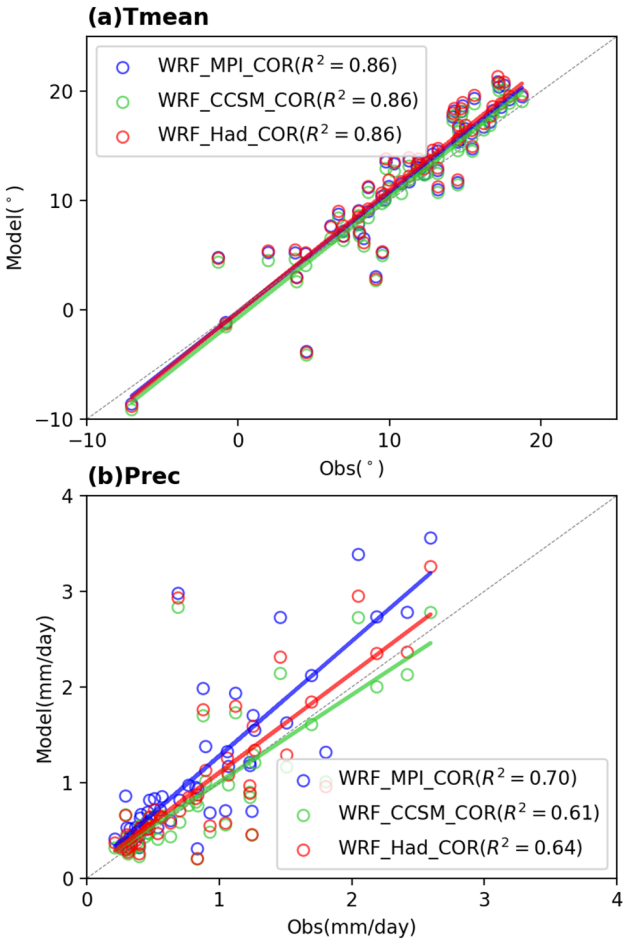

Fig. 6 Scatter plots of annual mean Tmean (**a**) and annual precipitation (Prec, **b**) between the station observation and the RCM outputs during the reference period

for spring and autumn in this study (Figs. 7, 8, and Fig. S7). The warming in summer has a west–east pattern (Fig. S7j-l). The enhanced warming in the northern part of CA from autumn to spring is mainly caused by less snow cover (see changes in snow depth in Fig. S8) and smaller albedo (Fig. S9) in these seasons in the future. On one hand, the local warming can accelerate the snow melting and shorten snow cover duration. On the other hand, enhanced warming in the Arctic from October to April, known as the Arctic amplification, can reduce meridional temperature gradients in the Northern Hemisphere, weaken mid-latitude westerly flow and cyclones, and decrease mid-latitude precipitation (Dai et al. 2019; Dai and Song 2020; Routson et al. 2019; Walsh 2014).

Numerous studies found that the warming rate in mountains is (will be) enhanced relative to non-mountain regions during the past (in the future), like the European Alps, the Tibetan Plateau/Himalayas in Asia and the Rocky Mountains in the United States (Palazzi et al. 2019; Pepin et al. 2015; Rangwala et al. 2013). However, our simulations show that the warming over the high-elevation regions in CA, especially in the Tien Shan, is generally lower than that over the plain areas (Fig. 7, see the results of subregion MT in Fig. 8, and Fig. S7), which is consistent with the analyses based on the reanalysis datasets during 1979–2011 (Hu et al. 1979). The possible reason why the enhanced warming projected in many mountains in the world is not detected in CA is that the important mechanisms that contribute towards elevation-dependent warming (EDW, Pepin et al. 2015), like snow albedo and surface-based feedbacks, are lacked in the Tien Shan and Pamirs, which is out of our scope in the current paper and needs further studies.

3.2.2 Projected changes in heatwave characteristics

To quantify changes in heatwave characteristics over a warmer CA in the near-term future, we differentiate heatwave day frequency (HWF), number (HWN) and maximum duration (HWD). All of these characteristics are expected to become more severe by 2031–2050 (Fig. 9). The frequency of heatwave days (HWF) strongly increases in the northeast and the very south (Fig. 9a). Averaged over CA, HWF changes from about 25 days per year (1986–2005) to around 45–55 days in 2031–2050 (Table 3, range depending on model). The average number of heatwaves (HWN) increases from 2.4 to 2.5 per year (1986–2005) to about 3–4 heatwaves per year (2031–2050). Moreover, simulated heatwaves are 1.5–1.9 times longer in the coming decades (2031–2050).

Changes in heatwave frequency and duration are mainly related to the mean warming in summer season. For instance, the WRF_Had_COR simulation depicts an increasing trend of warming from west to east (Fig. S7l) in summer, which is similar with the geographical pattern of HWF and HWD (Fig. S10c, i). This finding is consistent with the simulations in Europe (Fischer and Schär 2010). With different warming amplitude in summer, changes in the heatwave characteristics varies across the RCM simulations (Fig. S10), highlighting the necessity of using multiple GCMs as the lateral boundary conditions to give a range of the projected changes in CA.

3.2.3 Projected changes in drought indices

The RCM simulations commonly show that annual precipitation will slightly increase over most of the plain areas (see the slashed areas in Fig. 10a), with the ensemble-mean increase of 0.01 mm/day in CA. For SPI is calculated based on precipitation data, changes in annual mean SPI has a similar spatial pattern with those in precipitation (Fig. 10b vs Fig. 10a), with the ensemble-mean increase of 0.10. In terms of precipitation and SPI, a wetter condition is anticipated in CA during 2031–2050 relative to the reference period.

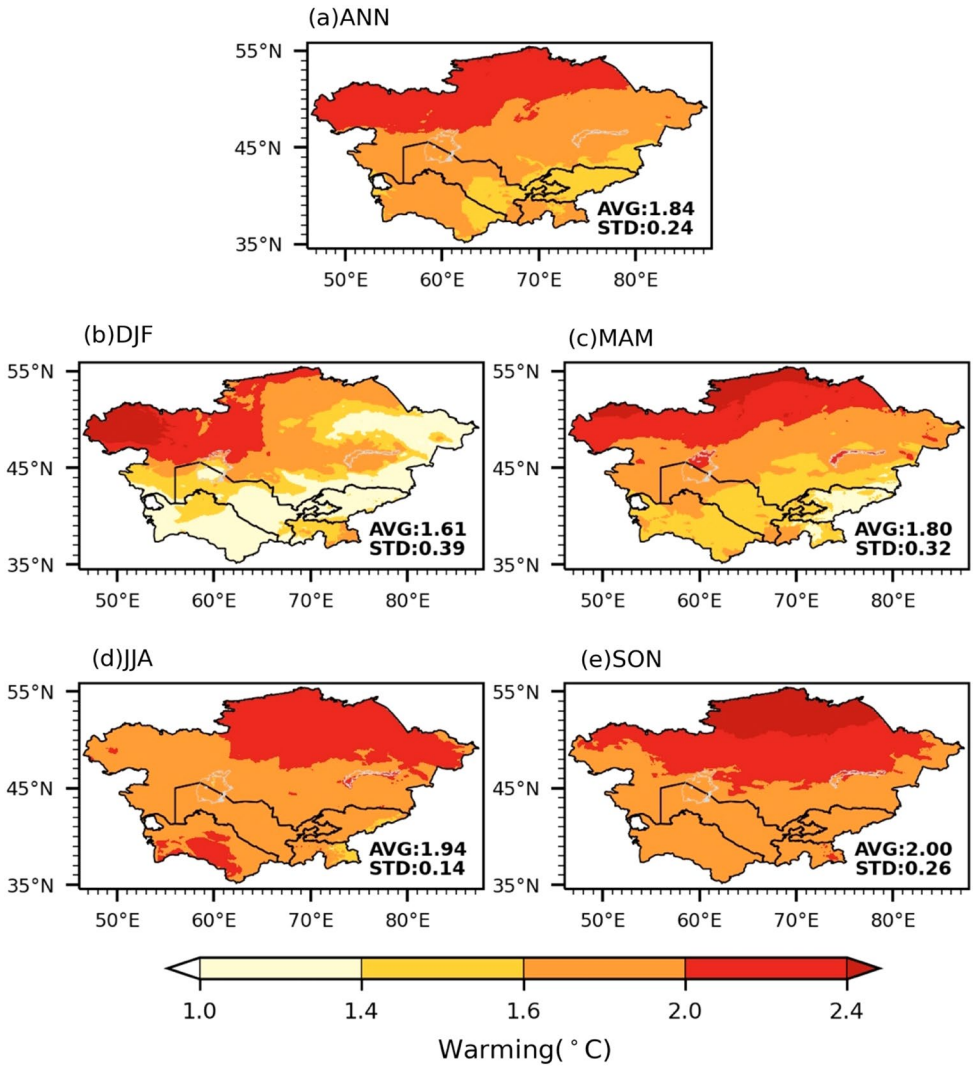

Fig. 7 Projected ensemble-mean changes of annual (ANN) and seasonal (DJF, December–January–February; MAM, March–April–May; JJA, June–July–August; SON, September–October–November) mean Tmean in Central Asia in the RCM simulations. Their regional mean (AVG) and standard deviation (STD) are listed

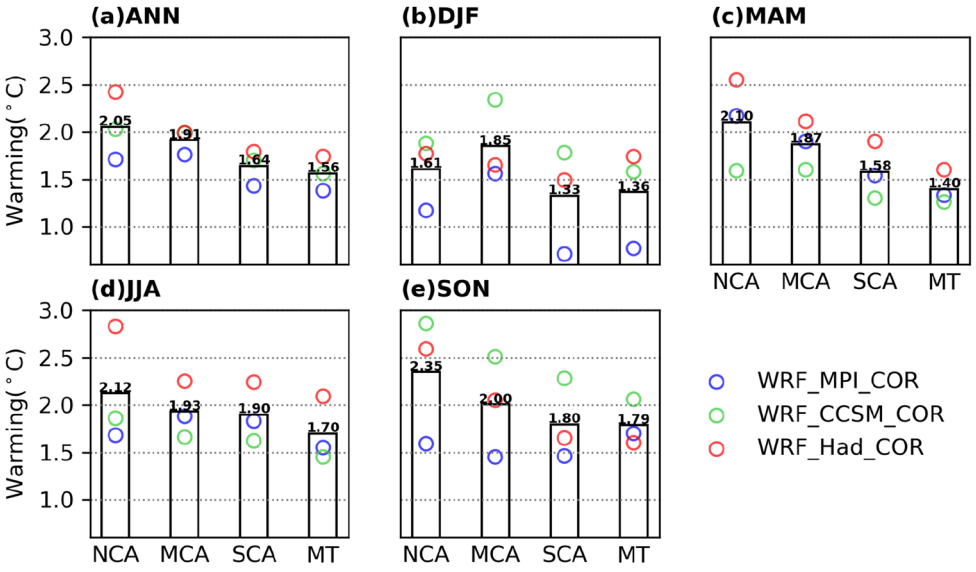

Fig. 8 Projected changes in annual and seasonal mean TG averaged over four climate sub-regions (NCA, MCA, SCA, and MT) in the RCM simulations. The markers indicate the results of each RCM simulation and the bars indicate the ensemble means

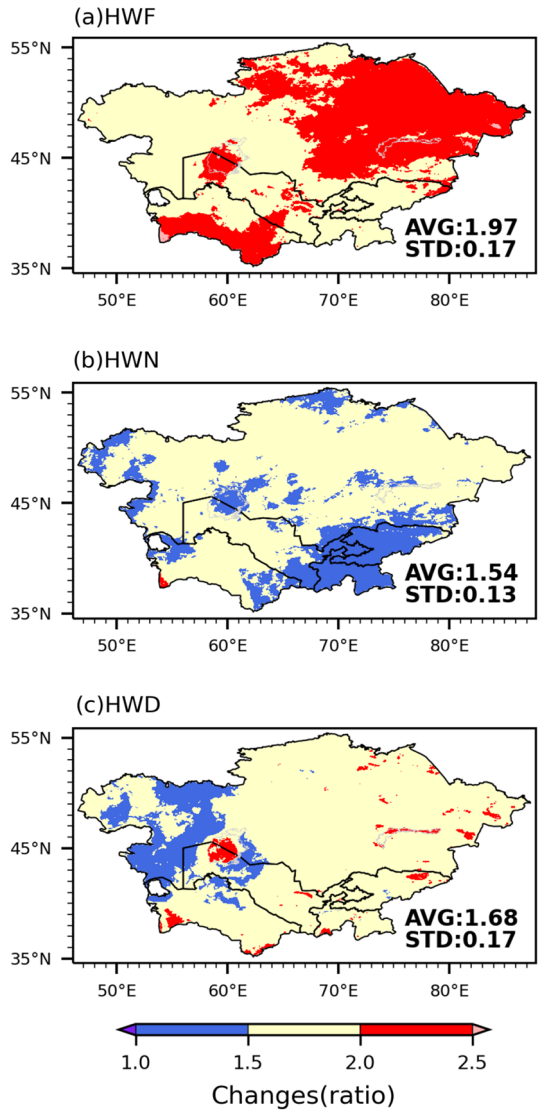

Fig. 9 Projected ensemble-mean changes of heatwave day frequency (HWF), number of heatwave (HWN), and heatwave maximum duration (HWD) in the RCM simulations. These indices are expressed as ratio between the future and reference period

However, the strong regional warming as discussed above will favor the increase of PET (0.32 mm/day, Fig. 10c), which can easily offset the increase in precipitation and enhance drought. Therefore, annual mean SPEI taking into account of both precipitation and PET will decrease by − 1.04 (Fig. 10d), which reveals a drier CA in the near-term future. Comparison of changes in SPI and SPEI (Fig. 10b vs Fig. 10d) suggests that the warming plays a major role in the evolution of drought in the drylands like CA by increasing PET and both temperature and precipitation should be taken into account to make a fairer assessment on the dry/wet change in these regions. We also calculated changes in these drought indices for each season, and the results (not shown) are consistent with those on the annual scale.

4 Summary

To project the regional climate in CA, bias-corrected multiple GCMs (MPI-ESM-MR, CCSM4, and HadGEM2-ES) from CMIP5 are selected to conduct high-resolution (9 km) dynamical downscaling over this area with the regional climate model WRF for the near-term future (2031–2050) relative to the reference period of 1986–2005, under the carbon emission scenario of RCP4.5.

Firstly, we carefully evaluated the RCM and GCM simulated daily temperature and precipitation. It's found that the high-resolution RCM outputs are excellent in describing the local temperature and precipitation in CA despite some systematic biases, and have numerous added values respect to the original GCMs, especially in the mountainous areas. Both the bias-correction method and dynamical downscaling method contribute to improving the RCM simulation. The former contributes more to reducing the biases of the climatology and the latter contributes more to capturing the spatial pattern.

Then, basic features of the projected climate changes across the RCM simulations are demonstrated. All the RCM simulations (MPI_WRF_COR, CCSM_WRF_COR, and

Table 3 Regional averages of the simulated heatwave indices

Region	CA	NCA	MCA	SCA	MT
HWF (days per year)					
1986–2005	25.1 (25.4/24.7)	23.9 (25.5/21.6)	25.1 (25.8/24.1)	25.2 (26.5/24.5)	27.5 (28.5/26.9)
2031–2050	48.7 (55.3/44.6)	49.2 (59.9/42.9)	48.3 (53.5/45.1)	49.1 (54.8/44.3)	48.2 (53.6/42.8)
HWN (heatwaves per year)					
1986–2005	2.4 (2.5/2.4)	2.4 (2.6/2.4)	2.4 (2.6/2.3)	2.4 (2.4/2.3)	2.4 (2.6/2.2)
2031–2050	3.7 (3.9/3.3)	3.9 (4.5/3.4)	3.7 (3.9/3.4)	3.6 (3.9/3.3)	3.1 (3.7/2.7)
HWD (days)					
1986–2005	13.6 (13.8/13.4)	12.3 (13.0/11.1)	13.4 (14.0/12.9)	14.2 (14.8/13.7)	15.9 (16.7/15.4)
2031–2050	23.1 (26.2/19.8)	21.9 (25.2/17.5)	22.3 (24.2/19.5)	24.2 (28.1/21.3)	27.6 (33.4/22.3)

The ensemble mean (first number) as well as the minimum and maximum ensemble member (in parentheses) are listed

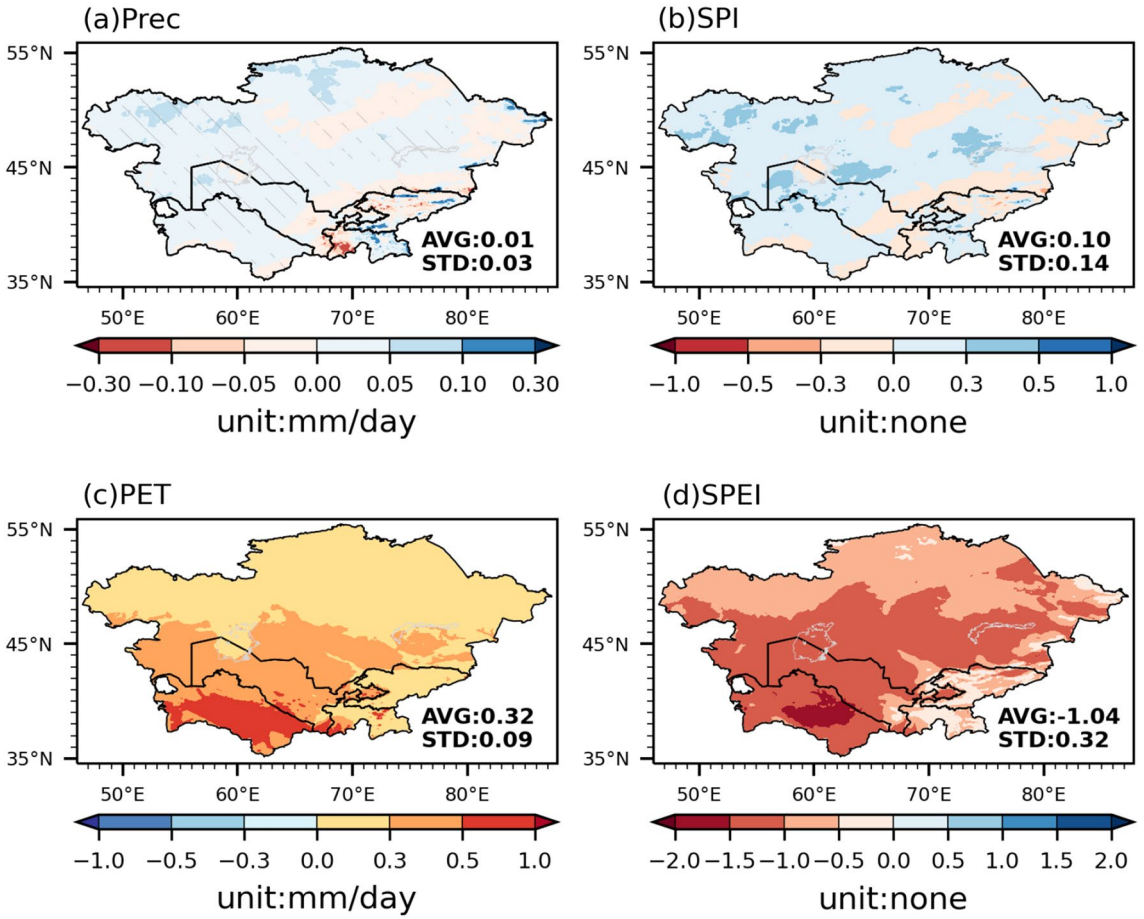

Fig. 10 Projected ensemble-mean changes of annual precipitation (Prec), annual mean Standardized Precipitation Index (SPI), potential evapotranspiration (PET), and Standardized Precipitation Evapotranspiration Index (SPEI) in the RCM simulations. The slashed areas in subplot a indicate where the signals (±) of the changes in the RCM simulations are consistent

Had_WRF_COR) show significant warming over CA in the near-term future, with the annual mean Tmean increase averaged over the entire area by 1.63, 1.89, and 2.01 ℃, respectively. They commonly reveal that the temperature will rise faster north of ~ 45 °N for each season except summer and the high-elevation areas generally have a weaker warming than the plains. Heatwave day frequency (HWF), number (HWN) and maximum duration (HWD) are expected to become more severe by 2031–2050. In terms of precipitation and SPI, a wetter condition is anticipated in CA in the coming decades. However, a fairer assessment of the dry/wet change in CA with SPEI which takes into account of both precipitation and PET reveals a drier condition.

With the limitation of the computational and time cost, this study used three GCMs from CMIP5 to do the dynamical downscaling over CA, which is an improvement compared to using single GCM. However, it still harbors uncertainties in the projected climate changes, especially for the extreme climate indices (i. e., changes in the heatwave indices as shown in Fig. S10). The downscaled results produced in this study provide high-resolution warming scenarios in CA, which is appropriate for the ecological and hydrological applications and will be published on National Tibetan Plateau/Third Pole Environment Data Center. The reason why the elevation-dependent warming is not detected in the high-elevation areas in CA will be explained, by calculating the partial temperature changes due to changes in different terms in surface energy budget.

Supplementary Information The online version contains supplementary material available at https://doi.org/10.1007/s00382-021-05934-2.

Acknowledgements This study was supported by the Strategic Priority Research Program of Chinese Academy of Sciences (Grand no. XDA20020201) and the General Project of the National Natural Science Foundation of China (Grand no. 41875134). In addition, we thank two anonymous reviewers for their helpful comments.

Author contributions All the authors except ZL made contributions to the conception or design of the work. YQ did the analyses and drafted the work and others except ZL revised it. ZL contributed to the collection of stations' data.

Funding This study was supported by the Strategic Priority Research Program of Chinese Academy of Sciences (Grand no. XDA20020201) and the General Project of the National Natural Science Foundation of China (Grand no. 41875134).

Availability of data and material The downscaled results produced in this study will be available at National Tibetan Plateau/Third Pole Environment Data Center (http://data.tpdc.ac.cn/en/).

Code availability The code used to correct the climatology of the global climate models is available at https://rda.ucar.edu/datasets/ds316.1/#!software. The python project used to calculate SPI and SPEI is available at https://github.com/monocongo/climate_indices.

Declarations

Conflicts of interest No conflicts of interests for authors.

References

Bruyère CL, Done JM, Holland GJ, Fredrick S (2014) Bias corrections of global models for regional climate simulations of high-impact weather. Clim Dyn 43:1847–1856. https://doi.org/10.1007/s00382-013-2011-6

Burunciuc L (2020) Natural disasters cost Central Asia $10 billion a year—are we doing enough to prevent them? World Bank Blogs

Chen L, Frauenfeld OW (2016) Impacts of urbanization on future climate in China. Clim Dyn 47:345–357. https://doi.org/10.1007/s00382-015-2840-6

Chen F, Wang J, Jin L, Zhang Q, Li J, Chen J (2009) Rapid warming in mid-latitude central Asia for the past 100 years. Front Earth Sci China 3:42. https://doi.org/10.1007/s11707-009-0013-9

Chen F, Huang W, Jin L, Chen J, Wang J (2011) Spatiotemporal precipitation variations in the arid Central Asia in the context of global warming. Sci China Earth Sci 54:1812–1821. https://doi.org/10.1007/s11430-011-4333-8

Dai A, Song M (2020) Little influence of Arctic amplification on mid-latitude climate. Nat Clim Chang 10:231–237. https://doi.org/10.1038/s41558-020-0694-3

Dai A, Luo D, Song M, Liu J (2019) Arctic amplification is caused by sea-ice loss under increasing CO2. Nat Commun 10:121. https://doi.org/10.1038/s41467-018-07954-9

Darmaraki S, Somot S, Sevault F, Nabat P, Cabos Narvaez WD, Cavicchia L, Djurdjevic V, Li L, Sannino G, Sein DV (2019) Future evolution of Marine Heatwaves in the Mediterranean Sea. Clim Dyn 53:1371–1392. https://doi.org/10.1007/s00382-019-04661-z

Dee DP, Uppala SM, Simmons A, Berrisford P, Poli P, Kobayashi S, Andrae U, Balmaseda M, Balsamo G, Bauer DP (2011) The ERA-Interim reanalysis: configuration and performance of the data assimilation system. Q J R Meteorol Soc 137:553–597

Done JM, Holland GJ, Bruyère CL, Leung LR, Suzuki-Parker A (2015) Modeling high-impact weather and climate: lessons from a tropical cyclone perspective. Clim Change 129:381–395. https://doi.org/10.1007/s10584-013-0954-6

Ehret U, Zehe E, Wulfmeyer V, Warrach-Sagi K, Liebert J (2012) HESS Opinions "Should we apply bias correction to global and regional climate model data?" Hydrol Earth Syst Sci 16:3391–3404. https://doi.org/10.5194/hess-16-3391-2012

Fischer EM, Schär C (2010) Consistent geographical patterns of changes in high-impact European heatwaves. Nat Geosci 3:398–403. https://doi.org/10.1038/ngeo866

Frenken K (2013) Irrigation in Central Asia in figures, Food and Agriculture Organization of the United Nations

Gabriel KA, Kimon K (2015) Analysis of scenarios integrating the INDCs, EUR - Scientific and Technical Research Reports

Gao X, Pal JS, Giorgi F (2016) Projected changes in mean and extreme precipitation over the Mediterranean region from a high resolution double nested RCM simulation. Geophys Res Lett 2016:33. https://doi.org/10.1029/2005GL024954

Gessner U, Naeimi V, Klein I, Kuenzer C, Klein D, Dech S (2013) The relationship between precipitation anomalies and satellite-derived vegetation activity in Central Asia. Glob Planet Change 110:74–87. https://doi.org/10.1016/j.gloplacha.2012.09.007

Harris I, Osborn TJ, Jones P, Lister D (2020) Version 4 of the CRU TS monthly high-resolution gridded multivariate climate dataset. Sci Data 7:109. https://doi.org/10.1038/s41597-020-0453-3

Hersbach H, Bell B, Berrisford P, Hirahara S, Horányi A, Muñoz-Sabater J, Nicolas J, Peubey C, Radu R, Schepers D, Simmons A, Soci C, Abdalla S, Abellan X, Balsamo G, Bechtold P, Biavati G, Bidlot J, Bonavita M, De Chiara G, Dahlgren P, Dee D, Diamantakis M, Dragani R, Flemming J, Forbes R, Fuentes M, Geer A, Haimberger L, Healy S, Hogan RJ, Hólm E, Janisková M, Keeley S, Laloyaux P, Lopez P, Lupu C, Radnoti G, de Rosnay P, Rozum I, Vamborg F, Villaume S, Thépaut J-N (2020) The ERA5 global reanalysis. Q J R Meteorol Soc 146:1999–2049. https://doi.org/10.1002/qj.3803

Hong S-Y, Noh Y, Dudhia J (2006) A new vertical diffusion package with an explicit treatment of entrainment processes. Mon Wea Rev 134:2318–2341. https://doi.org/10.1175/MWR3199.1

Hu Z, Zhang C, Hu Q, Tian H (2014) Temperature changes in Central Asia from 1979 to 2011 based on multiple datasets. J Clim 27:1143–1167. https://doi.org/10.1175/jcli-d-13-00064.1

Huang A, Zhou Y, Zhang Y, Huang D, Zhao Y, Wu H (2014) Changes of the annual precipitation over central asia in the twenty-first century projected by multimodels of CMIP5. J Clim 27:6627–6646. https://doi.org/10.1175/jcli-d-14-00070.1

Iacono MJ, Delamere JS, Mlawer EJ, Shephard MW, Clough SA, Collins WD (2008) Radiative forcing by long-lived greenhouse gases: calculations with the AER radiative transfer models. J Geophys Res Atmos 2008:113. https://doi.org/10.1029/2008JD009944

Jayasankar CB, Rajendran K, Surendran S (2018) Monsoon climate change projection for the orographic west coast of India using high-resolution nested dynamical downscaling model. J Geophys Res Atmos 123:7821–7838. https://doi.org/10.1029/2018JD028677

Jiang J, Zhou T, Zhang W (2019) Evaluation of satellite and reanalysis precipitable water vapor data sets against radiosonde observations in Central Asia. Earth Space Sci 6:1129–1148. https://doi.org/10.1029/2019EA000654

Jiang J, Zhou T, Chen X, Zhang L (2020a) Future changes in precipitation over Central Asia based on CMIP6 projections. Environ Res Lett 15:054009. https://doi.org/10.1088/1748-9326/ab7d03

Jiang Q, Li W, Fan Z, He X, Sun W, Chen S, Wen J, Gao J, Wang J (2020b) Evaluation of the ERA5 reanalysis precipitation dataset over Chinese Mainland. J Hydrol 2020:125660. https://doi.org/10.1016/j.jhydrol.2020.125660

Jing X, Xue L, Yin Y, Yang J, Steinhoff DF, Monaghan A, Yates D, Liu C, Rasmussen R, Taraphdar S, Pauluis O (2020) Convection-permitting regional climate simulations in the arabian gulf region using WRF driven by bias-corrected GCM data. J Clim 33:7787–7815. https://doi.org/10.1175/jcli-d-20-0155.1

Kim G, Cha D-H, Park C, Jin C-S, Lee D-K, Suh M-S, Oh S-G, Hong S-Y, Ahn J-B, Min S-K, Kang H-S (2021) Evaluation and projection of regional climate over East Asia in CORDEX-East Asia phase I experiment. Asia-Pac J Atmos Sci 57:119–134. https://doi.org/10.1007/s13143-020-00180-8

Komurcu M, Emanuel KA, Huber M, Acosta RP (2018) High-resolution climate projections for the Northeastern United States using dynamical downscaling at convection-permitting scales. Earth Space Sci 5:801–826. https://doi.org/10.1029/2018EA000426

Kumar D, Dimri AP (2018) Regional climate projections for Northeast India: an appraisal from CORDEX South Asia experiment. Theor Appl Climatol 134:1065–1081. https://doi.org/10.1007/s00704-017-2318-z

Liang X-Z, Kunkel KE, Meehl GA, Jones RG, Wang JXL (2008) Regional climate models downscaling analysis of general circulation models present climate biases propagation into future change projections. Geophys Res Lett 2008:35. https://doi.org/10.1029/2007GL032849

Luo M, Feng JM, Xu ZF, Chen L, Wang J, Wang YL, Lin S, Zhong LH (2020) Decadal wintertime temperature changes in East Asia During 1958–2001 and the contributions of internal variability and external forcing. J Geophys Res Atmos 125:e2019JD031840. https://doi.org/10.1029/2019jd031840

Mannig B, Müller M, Starke E, Merkenschlager C, Mao W, Zhi X, Podzun R, Jacob D, Paeth H (2013) Dynamical downscaling of climate change in Central Asia. Glob Planet Change 110:26–39. https://doi.org/10.1016/j.gloplacha.2013.05.008

McKee TB, Doesken NJ, Kleist J (1993) The relationship of drought frequency and duration to time scales. In: Preprints, Eighth Conf. on Applied Climatology, Anaheim, CA, Amer. Meteor. Soc., pp 179–184

Narama C, Kääb A, Duishonakunov M, Abdrakhmatov K (2010) Spatial variability of recent glacier area changes in the Tien Shan Mountains, Central Asia, using Corona (~ 1970), Landsat (~ 2000), and ALOS (~ 2007) satellite data. Glob Planet Change 71:42–54

Niu G-Y, Yang Z-L, Mitchell KE, Chen F, Ek MB, Barlage M, Kumar A, Manning K, Niyogi D, Rosero E, Tewari M, Xia Y (2011) The community Noah land surface model with multiparameterization options (Noah-MP): 1. Model description and evaluation with local-scale measurements. J Geophys Res Atmos 2011:116. https://doi.org/10.1029/2010JD015139

Niu X, Wang S, Tang J, Lee D-K, Gutowski W, Dairaku K, McGregor J, Katzfey J, Gao X, Wu J, Hong S-Y, Wang Y, Sasaki H, Fu C (2018) Ensemble evaluation and projection of climate extremes in China using RMIP models. Int J Climatol 38:2039–2055. https://doi.org/10.1002/joc.5315

Ortiz LE, González JE, Horton R, Lin W, Wu W, Ramamurthy P, Arend M, Bornstein RD (2019) High-resolution projections of extreme heat in New York City. Int J Climatol 39:4721–4735. https://doi.org/10.1002/joc.6102

Ozturk T, Turp MT, Türkeş M, Kurnaz ML (2017) Projected changes in temperature and precipitation climatology of Central Asia CORDEX Region 8 by using RegCM4.3.5. Atmos Res 183:296–307. https://doi.org/10.1016/j.atmosres.2016.09.008

Palazzi E, Mortarini L, Terzago S, von Hardenberg J (2019) Elevation-dependent warming in global climate model simulations at high spatial resolution. Clim Dyn 52:2685–2702. https://doi.org/10.1007/s00382-018-4287-z

Peng D, Zhou T, Zhang L, Zou LJCD (2019) Detecting human influence on the temperature changes in Central. Asia 53:4553–4568

Pepin N, Bradley RS, Diaz HF, Baraer M, Caceres EB, Forsythe N, Fowler H, Greenwood G, Hashmi MZ, Liu XD, Miller JR, Ning L, Ohmura A, Palazzi E, Rangwala I, Schöner W, Severskiy I, Shahgedanova M, Wang MB, Williamson SN, Yang DQ, Mountain Research Initiative, E. D. W. W. G. (2015) Elevation-dependent warming in mountain regions of the world. Nature Clim Change 5:424–430. https://doi.org/10.1038/nclimate2563

Poornima S, Pushpalatha M (2019) Drought prediction based on SPI and SPEI with varying timescales using LSTM recurrent neural network. Soft Comput 23:8399–8412. https://doi.org/10.1007/s00500-019-04120-1

Qiu Y, Hu Q, Zhang C (2017) WRF simulation and downscaling of local climate in Central Asia. Int J Climatol 37:513–528. https://doi.org/10.1002/joc.5018

Rangwala I, Sinsky E, Miller JR (2013) Amplified warming projections for high altitude regions of the northern hemisphere mid-latitudes from CMIP5 models. Environ Res Lett 8:024040. https://doi.org/10.1088/1748-9326/8/2/024040

Routson CC, McKay NP, Kaufman DS, Erb MP, Goosse H, Shuman BN, Rodysill JR, Ault T (2019) Mid-latitude net precipitation decreased with Arctic warming during the Holocene. Nature 568:83–87. https://doi.org/10.1038/s41586-019-1060-3

Seddon AW, Macias-Fauria M, Long PR, Benz D, Willis KJ (2016) Sensitivity of global terrestrial ecosystems to climate variability. Nature 531:229–232

Skamarock WC, Klemp JB, Dudhia J, Gill DO, Barker DM, Wang W, Powers JG (2008) A description of the Advanced Research WRF version 3. In: NCAR Technical note-475+ STR

Sorg A, Bolch T, Stoffel M, Solomina O, Beniston M (2012) Climate change impacts on glaciers and runoff in Tien Shan (Central Asia). Nat Clim Change 2:725–731

Supari A, Tangang F, Juneng L, Cruz F, Chung JX, Ngai ST, Salimun E, Mohd MSF, Santisirisomboon J, Singhruck P, PhanVan T, Ngo-Duc T, Narisma G, Aldrian E, Gunawan D, Sopaheluwakan A (2020) Multi-model projections of precipitation extremes in Southeast Asia based on CORDEX-Southeast Asia simulations. Env Res 184:109350. https://doi.org/10.1016/j.envres.2020.109350

Thompson G, Eidhammer T (2014) A study of aerosol impacts on clouds and precipitation development in a large winter cyclone. J Atmos Sci 71:3636–3658. https://doi.org/10.1175/jas-d-13-0305.1

Thornthwaite CW (1948) An approach toward a rational classification of climate. Geogr Rev 38:55–94. https://doi.org/10.2307/210739

Thurman M (2011) Natural disaster risks in Central Asia: a synthesis, UNDP/BCPR, Regional Disaster Risk Reduction Asvisor, Europe and CIS

Vicente-Serrano SM, Beguería S, López-Moreno JI (2010) A multiscalar drought index sensitive to global warming: the standardized precipitation evapotranspiration index. J Clim 23:1696–1718. https://doi.org/10.1175/2009jcli2909.1

Walsh JE (2014) Intensified warming of the Arctic: causes and impacts on middle latitudes. Glob Planet Change 117:52–63. https://doi.org/10.1016/j.gloplacha.2014.03.003

Wang J, Chen Y, Tett SFB, Yan Z, Zhai P, Feng J, Xia J (2020a) Anthropogenically-driven increases in the risks of summertime compound hot extremes. Nat Commun 11:528. https://doi.org/10.1038/s41467-019-14233-8

Wang Y, Feng J, Luo M, Wang J, Qiu Y (2020b) Uncertainties in simulating central Asia: sensitivity to physical parameterizations using Weather Research and Forecasting model. Int J Climatol 40:5813–5828. https://doi.org/10.1002/joc.6567

Wei K, Wang L (2013) Reexamination of the aridity conditions in arid Northwestern China for the last decade. J Clim 26:9594–9602. https://doi.org/10.1175/jcli-d-12-00605.1

Xu Z, Yang Z-L (2012) An improved dynamical downscaling method with GCM bias corrections and its validation with 30 years of climate simulations. J Clim 25:6271–6286. https://doi.org/10.1175/JCLI-D-12-00005.1

Yu S, Yan Z, Freychet N, Li Z (2020) Trends in summer heatwaves in central Asia from 1917 to 2016: association with large-scale atmospheric circulation patterns. Int J Climatol 40:115–127. https://doi.org/10.1002/joc.6197

Zhang C, Wang Y, Hamilton K (2011) Improved representation of boundary layer clouds over the southeast pacific in ARW-WRF using a modified Tiedtke Cumulus parameterization

scheme. Mon Wea Rev 139:3489–3513. https://doi.org/10.1175/mwr-d-10-05091.1

Zhang C, Lu D, Chen X, Zhang Y, Maisupova B, Tao Y (2016) The spatiotemporal patterns of vegetation coverage and biomass of the temperate deserts in Central Asia and their relationships with climate controls. Remote Sens Environ 175:271–281. https://doi.org/10.1016/j.rse.2016.01.002

Zhu X, Wei Z, Dong W, Ji Z, Wen X, Zheng Z, Yan D, Chen D (2020) Dynamical downscaling simulation and projection for mean and extreme temperature and precipitation over central Asia. Clim Dyn. https://doi.org/10.1007/s00382-020-05170-0

Zittis G, Hadjinicolaou P, Klangidou M, Proestos Y, Lelieveld J (2019) A multi-model, multi-scenario, and multi-domain analysis of regional climate projections for the Mediterranean. Reg Environ Change 19:2621–2635. https://doi.org/10.1007/s10113-019-01565-w

Zou L, Zhou T (2016) Future summer precipitation changes over CORDEX-East Asia domain downscaled by a regional ocean-atmosphere coupled model: a comparison to the stand-alone RCM. J Geophys Res Atmos 121:2691–2704. https://doi.org/10.1002/2015JD024519

Zou L, Zhou T (2017) Dynamical downscaling of East Asian winter monsoon changes with a regional ocean–atmosphere coupled model. Q J R Meteorol Soc 143:2245–2259. https://doi.org/10.1002/qj.3082